JACS
JOURNAL OF THE AMERICAN CHEMICAL SOCIETY
Communication
pubs.acs.org/JACS

Ferrous Centers Confined on Core–Shell Nanostructures for Low-Temperature CO Oxidation

Xiaoguang Guo,[†] Qiang Fu,*[,†] Yanxiao Ning,[†] Mingming Wei,[†] Mingrun Li,[†] Shuo Zhang,[‡] Zheng Jiang,[‡] and Xinhe Bao*[,†]

[†]State Key Laboratory of Catalysis, Dalian Institute of Chemical Physics, Chinese Academy of Sciences, Dalian 116023, P. R. China
[‡]Shanghai Synchrotron Radiation Facility, Shanghai Institute of Applied Physics, Chinese Academy of Sciences, Shanghai 201204, P. R. China

Supporting Information

ABSTRACT: A noble metal (NM) can stabilize monolayer-dispersed surface oxide phases with metastable nature. The formed "oxide-on-metal" inverse catalyst presents better catalytic performance than the NM because of the introduction of coordinatively unsaturated cations at the oxide–metal boundaries. Here we demonstrate that an ultrathin NM layer grown on a non-NM core can impose the same constraint on the supported oxide as the bulk NM. Cu@Pt core–shell nanoparticles (NPs) decorated with FeO patches use much less Pt but exhibit performance similar to that of Pt NPs covered with surface FeO patches in the catalytic oxidation of CO. The "oxide-on-core@shell" inverse catalyst system may open a new avenue for the design of advanced nanocatalysts with decreased usage of noble metals.

Many industrial catalysts consist of noble metal (NM) nanoparticles (NPs) supported on a transition metal oxide (TMO), in which the metal is the primary active component. However, the oxide, particularly a reducible oxide such as TiO_2, Fe_2O_3, or CeO_2, may not only act as a support for the dispersion of metal NPs but also promote the metal-catalyzed reactions.[1] The important role of the oxide support and metal–oxide interface in surface reactions has been extensively studied and is highlighted by the "strong metal–support interaction" (SMSI) concept.[2] It has long been recognized that in the SMSI state, the oxide close to the metal–oxide boundary often becomes defective, which contributes to the promotional effect of the oxide support.[1−3]

To make use of metal–oxide interfaces in surface reactions, nanostructured TMOs can be constructed on NMs, forming "oxide-on-metal" inverse catalysts (Scheme 1).[4] Therein, the supported TMO is often monolayer-dispersed and metastable because of the constraint imposed by the NM surface.[4,5] TM atoms at the peripheries of the supported two-dimensional (2D) oxide nanoislands are coordinatively unsaturated and thus highly active for many reactions.[6,7] For example, we have demonstrated that a Pt surface decorated with monolayer-dispersed FeO nanoislands is much more active than a pure Pt surface in CO oxidation at low temperature. The coordinatively unsaturated ferrous (CUF) atoms confined at the peripheries of the 2D FeO nanoislands help to activate O_2 and alleviate CO poisoning.[4b,7] Similar "oxide-on-Pt" structural configurations have been successfully built in "NiO-on-Pt" and "CoO-on-Pt" systems.[4a,8] A general interface confinement effect between TMOs and NMs that enhances the catalytic performance of the NMs via introduction of the coordinatively unsaturated (CUS) cations at the oxide–metal boundaries has been established.

Scheme 1. Various Structural Configurations of Supported NP Catalysts: (A) Noble Metal NP; (B) "TMO-on-NM" NP Consisting of a Noble Metal NP Decorated with Surface TM Oxide; (C) "TMO-on-NM Shell" NP with TM Oxide Decorating the Surface of a Core–Shell NP

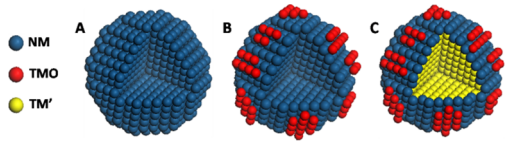

Since NMs are expensive and scarce, further effort to reduce their use in inverse catalysts is needed. It is known that the construction of non-NM@NM core–shell nanostructures has been regarded as an effective way to use NMs efficiently.[9] Core–shell NPs containing TM cores and Pt shells have been widely used as catalysts for the oxygen reduction reaction (ORR), hydrogenation, dehydrogenation, the water-gas shift reaction, and preferential oxidation of CO in excess H_2 (PROX).[9,10] Motivated by these results, we suggest that an ultrathin Pt structure may be applied to stabilize monolayer-dispersed TMO patches. Consequently, the "oxide-on-NM" configuration can be converted into the "oxide-on-NM shell" system, which uses much less NM (Scheme 1).

In this communication, the "oxide-on-NM shell" scenario is successfully exemplified by "FeO-on-Cu@Pt" catalytic system. Cu@Pt core–shell NPs decorated with surface FeO patches show much higher activity for PROX than pure Pt NPs and are comparable to the "FeO-on-Pt" NP catalyst. The high efficiency of the "FeO-on-Cu@Pt" catalyst indicates that the ultrathin NM layer can stabilize coordinatively unsaturated cations on its surface. The "oxide-on-core@shell" catalytic system may open a new avenue for the design of advanced nanocatalysts with decreased usage of NMs.

Cu@Pt core–shell NPs were prepared by a sequential polyol process. First, $Cu(acac)_2$ (acac = acetylacetonate) was reduced

Received: April 23, 2012
Published: July 19, 2012

dx.doi.org/10.1021/ja3038883 | J. Am. Chem. Soc. 2012, 134, 12350–12353

in ethylene glycol (EG) at 198 °C in the presence of polyvinylpyrrolidine (PVP). Transmission electron microscopy (TEM) images of the resulting Cu colloids indicated that the Cu NPs had an average size of ~3.8 nm (Figure S1A in the Supporting Information). Subsequently, $PtCl_2$ was added to the Cu/EG colloids at 130 °C under an Ar atmosphere. The coating of Pt led to a slight increase in the particle size to 4.5 nm (Figure S1B). For comparison, Pt and PtCu alloy NPs of similar size were synthesized via reduction of $Pt(acac)_2$ and coreduction of $Cu(acac)_2$ and $Pt(acac)_2$, respectively (Figure S1C,D).

The obtained monometallic and bimetallic colloids were supported on carbon black (CB), producing Pt/CB, Cu/CB, Cu@Pt/CB, and PtCu/CB catalysts. Among them, the Cu@Pt and Pt NPs were further decorated with Fe through the reductive deposition precipitation (RDP) process,[11] forming Cu@Pt–Fe/CB and Pt–Fe/CB catalysts. All of the resulting catalysts were subjected to reduction in H_2 at 250 °C for 2 h and subsequently exposed to air slowly at room temperature. Scanning TEM (STEM) measurements clearly identified the supported metal NPs. Elemental mapping images showed that Pt, Cu, and Fe presented the same spatial distribution over the catalyst (Figure S2).

The X-ray diffraction (XRD) pattern of the Cu/CB sample indicated the presence of Cu and Cu_2O phases, with main peaks at 43.3° and 36.4°, respectively (Figure 1A). It is known

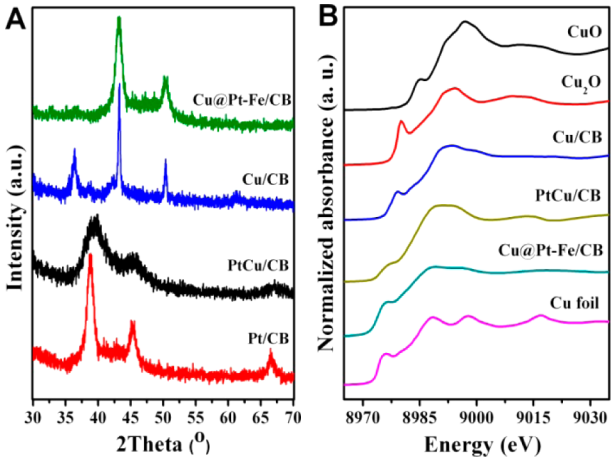

Figure 1. (A), XRD patterns of Cu@Pt–Fe/CB, Cu/CB, PtCu/CB, and Pt/CB samples. (B) Cu K-edge XANES spectra acquired from CuO and Cu_2O standards and Cu foil, Cu/CB, Cu@Pt–Fe/CB, and PtCu/CB samples.

that Cu surfaces are prone to oxidation in O_2.[12] When the Cu NPs are exposed to air at room temperature, the surface layers get oxidized while the core regions remain metallic because of the kinetic limit of surface oxidation. A complete Pt shell layer on the Cu@Pt core–shell NP may protect the Cu core against surface oxidation. Indeed, we observed only diffraction peaks of the metallic Cu phase in the XRD pattern of the Cu@Pt–Fe/CB sample. Complementary high-resolution TEM characterization showed that the core of each Cu@Pt–Fe NP was dominated by the face-centered cubic Cu structure, with an interlayer spacing of 0.21 nm (Figure S2). For the PtCu/CB sample, the main peak position shifted to a higher 2θ position by 0.9° relative to that of the Pt/CB sample as a result of alloying.[13]

Cu K-edge X-ray absorption near-edge structure (XANES) spectra of the Cu-containing catalysts were also acquired (Figure 1B). For comparison, CuO and Cu_2O standards and Cu foil were investigated under the same measurement conditions.[14] The Cu K-edge (k^3-weighted) Fourier transform is displayed in Figure S3. The main features in the spectra of the Cu@Pt–Fe/CB sample are similar to those of the Cu foil, again indicating that Cu in the core–shell nanostructures had a metallic nature because of the passivation of the Cu cores by the Pt shells. However, the characteristic peaks in the K-edge spectra of the Cu/CB and PtCu/CB samples lie between those of Cu foil and Cu_2O. Apparently, some of the Cu atoms were located at the surfaces of the Cu and PtCu NPs and become oxidized when exposed to air at room temperature. Cu atoms inside the NPs remained metallic. Therefore, the K-edge structures of the two samples contain the absorption characters of both Cu^0 and Cu^{1+} species. No Cu^{2+} species were observed in any of the samples.

Non-NM atoms outside Pt-based multimetallic NPs can be dissolved in dilute nitric acid, while those protected by the Pt shell or Pt skin structures remain unaffected.[4a,8b,15] On the contrary, a strong acid such as aqua regia can dissolve all metals no matter which structure the particles have. All of the supported catalysts were treated in both acid solutions, and the leached metal amounts were determined by inductively coupled plasma atomic emission spectrometry (ICP-AES) (Table 1).

Table 1. Amounts of Cu, Pt, and Fe Ions Leached from the Different Catalysts by 30 mmol/L HNO_3 and Aqua Regia Solutions, As Determined by ICP-AES[a]

	HNO_3			aqua regia		
catalyst[b]	Fe	Cu	Pt	Fe	Cu	Pt
Cu/CB	–	1.04	–	–	1.13	–
PtCu/CB	–	0.06	0.00	–	0.31	1.01
Cu@Pt/CB	–	0.00	0.00	–	1.10	0.91
Cu@Pt–Fe/CB	0.10	0.0	0.00	0.10	1.10	0.91
Cu@Pt/CB[c]	–	0.01	0.00	–	–	–
Cu@Pt–Fe/CB[c]	0.10	0.00	0.00	–	–	–

[a]The contents are reported in units of grams per 100 g of CB support. [b]All of the catalysts were reduced in flowing H_2 at 250 °C for 2 h and slowly exposed to air at room temperature. [c]This catalyst was additionally subjected to the PROX reaction from 27 to 250 °C at a ramp rate of 1 °C/min and subsequently exposed to air at room temperature.

The results showed that most of the Cu in the Cu/CB sample was leached in a 30 mmol/L HNO_3 solution. There was also a substantial amount of Cu (~19%) washed away from the PtCu/CB sample by the acid solution. However, no Cu was removed from the Cu@Pt/CB and Cu@Pt–Fe/CB samples, indicating that the Cu cores were completely coated by Pt shells. When aqua regia was used, all of the metals were dissolved, and the metal loadings were determined accordingly: 1.1 wt % Cu and 0.9 wt % Pt in the Cu@Pt/CB and Cu@Pt–Fe/CB samples, 1.0 wt % Pt and 0.3 wt % Cu in the PtCu/CB sample, and 1.1 wt % Cu in the Cu/CB sample.

The Cu/CB, PtCu/CB, Cu@Pt/CB, and 4 wt % Pt/CB catalysts were subjected to the PROX reaction (1% CO, 0.5% O_2, 50% H_2, and 48.5% He; 30 000 mL g^{-1} h^{-1}). CO conversion data from the temperature-programmed reactions are shown in Figure 2A, and the corresponding selectivity and O_2 conversion results are given in Figure S4. It can be seen that

dx.doi.org/10.1021/ja3038883 | J. Am. Chem. Soc. 2012, 134, 12350–12353

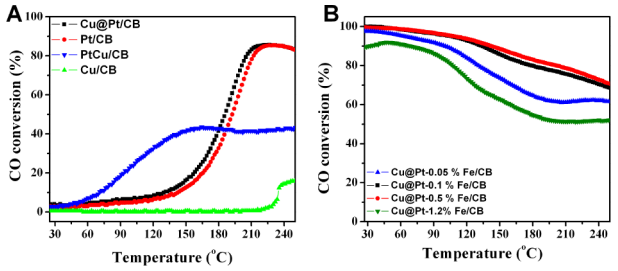

Figure 2. (A) Temperature-dependent CO conversion in PROX over the Cu@Pt/CB, Pt/CB, PtCu/CB, and Cu/CB catalysts. (B) Temperature-dependent CO conversion in PROX over the Cu@Pt/CB catalysts decorated with various amounts of Fe. The space velocity was 30 000 mL g^{-1} h^{-1}.

all of the catalysts exhibited very low CO and O_2 conversion at room temperature. Among them, PtCu alloy NPs showed a CO oxidation onset at 50 °C, but the maximum CO conversion was only 40%. With the Cu@Pt/CB catalyst, CO conversion started to increase above 100 °C and reached a maximum (85%) at 215 °C, which is similar to that of the Pt/CB catalyst. In our previous works, no significant improvement in the CO oxidation activity was observed over Pt-surface-rich catalysts with Fe or Ni in the subsurface regions.[4a,15a] These results indicate that the 3D-TM@Pt core−shell structure is not a highly active phase in PROX.

The PROX activity was significantly improved after the Cu@Pt NPs were decorated with Fe. Various Fe loadings were deposited on the Cu@Pt/CB samples. Relative to the Cu@Pt/CB catalyst, the resulting Cu@Pt−Fe/CB catalysts showed much higher CO conversion, particularly in the low-temperature regime (Figure 3B); 100% CO conversion was observed

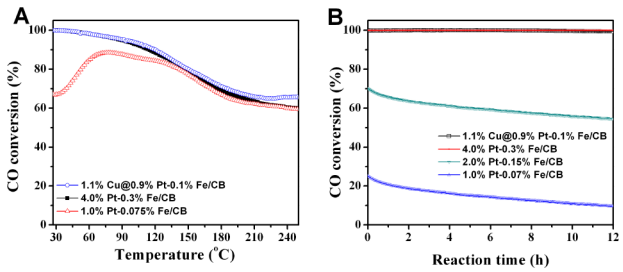

Figure 3. (A) Temperature-dependent CO conversion of PROX over the 1.1 wt % Cu@0.9 wt % Pt−0.1 wt % Fe/CB, 4 wt % Pt−0.3 wt % Fe/CB, and 1 wt % Pt−0.075 wt % Fe/CB catalysts. The space velocity was 30 000 mL g^{-1} h^{-1}. (B) Time-dependent CO conversion of PROX over the catalysts. The space velocity was 75 000 mL g^{-1} h^{-1}. The corresponding O_2 conversion is shown in Figure S6.

at room temperature with Fe loadings of 0.1 and 0.5 wt %. At high temperature, oxidation of H_2 may take place,[7] resulting in a decrease in the CO conversion because of the stoichiometric mixture of CO and O_2. Over the entire temperature range, the O_2 conversions remained nearly 100% (Figure S4). It should be noted that deposition of the same amount of Fe on the PtCu/CB and Cu/CB catalysts did not improve the PROX reaction performance very much (Figure S5).

Under the same reaction conditions, the Cu@Pt−Fe/CB (1.1 wt % Cu, 0.9 wt % Pt, and 0.1 wt % Fe) and Pt−Fe/CB (4 wt % Pt, 0.3 wt % Fe) catalysts presented comparable performance (Figure 3A and Figure S6). However, the Pt loading was decreased by a factor of 4 using the core−shell nanostructure. For comparison, the Pt loading in the Pt−Fe/CB catalyst was decreased to 1 wt %, similar to that in the Cu@Pt−Fe/CB catalyst. In this case, the PROX activity was much lower, with a CO conversion of 67% at room temperature (Figure 3A). At a higher space velocity (i.e., 75 000 mL g^{-1} h^{-1}), the CO conversion over the 1.0 wt % Pt−0.075 wt % Fe/CB catalyst at room temperature was 25% initially and decreased with time (Figure 3B). The 2.0 wt % Pt−0.15 wt % Fe/CB catalyst had a CO conversion of 70%. In contrast, the Cu@Pt−0.1% Fe/CB and 4 wt % Pt−0.3 wt % Fe/CB catalysts exhibited 100% CO conversion. No loss of activity was observed during reaction for 12 h.

On the basis of the average size of the Cu NPs (Figure S1A) and the relative weights of Cu and Pt in the Cu@Pt NPs (Table 1), the coverage of the Pt shell on the Cu core was calculated to be ∼1.4 monolayer (ML), assuming a simple cubic shape for the NPs. The increase in the particle size due to coating of the Cu NPs with Pt (from 3.8 to 4.5 nm; Figure S1) also confirmed the ultrathin Pt shell structure. After the Cu@Pt and Cu@Pt−Fe catalysts were reduced in H_2 at 250 °C and subsequently subjected to the PROX reaction from room temperature to 250 °C, little Cu was removed in the leaching process (Table 1). Therefore, the Cu@Pt core−shell structure was well-maintained during the reduction and reaction processes. For the Cu@Pt−Fe/CB sample, the leaching experiment indicated that almost all of Fe species were outside the NP shells (Table 1). In the RDP process, the reduction of Fe ions must be facilitated by the Pt surface, and the deposited Fe should stay exclusively on the Pt surface. Similarly, according to the average size of the Cu@Pt NPs and the Fe loading (0.1 wt %), the coverage of surface Fe on the Cu@Pt NP surface was estimated to be ∼0.33 ML, which is similar to the value of 0.28 ML determined by CO chemisorption over the Cu@Pt/CB and Cu@Pt−Fe/CB catalysts. According to this discussion, we can conclude that the "Fe(or FeOx)-on-Cu@Pt" surface architecture was established and well-maintained during the reaction.

To determine the chemical state of the surface Fe species under the PROX reaction conditions, the Cu@Pt−Fe/CB sample was investigated by in situ XANES (Figure 4). The Fe K-edge of the operating Cu@Pt−Fe/CB sample at room temperature was between those in the spectra of Fe foil and an Fe_2O_3 standard. This result confirms that the metallic Fe in the reduced Cu@Pt−Fe/CB sample was transformed into ferrous species in PROX, as in the Pt−Fe catalytic system.[7] The FeO surface structure was stabilized by the confinement effect at the

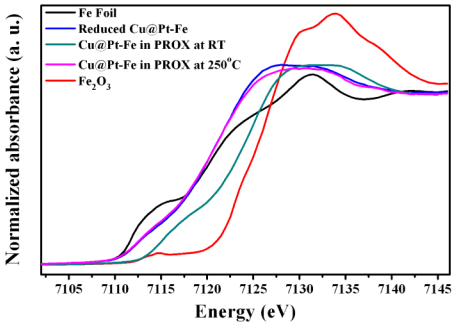

Figure 4. In-situ Fe K-edge XANES spectra of the Cu@Pt−Fe/CB catalyst reduced in H_2 (10% H_2, 90% He; 30 mL/min) at 250 °C for 40 min and subjected to PROX (1% CO, 0.5% O_2, 10% H_2, 88.5% He; 30 mL/min) at room temperature for 20 min and at 250 °C for 20 min. The spectra of Fe foil and an Fe_2O_3 standard are also included.

dx.doi.org/10.1021/ja3038883 | J. Am. Chem. Soc. 2012, 134, 12350−12353

oxide−Pt interface. The interface confinement effect was also illustrated by research on a model system in which monolayer FeO nanoislands were stabilized by the Pt skin grown on a Cu(111) surface (Figure S7). The in situ study also indicated that FeO was reduced back to the metallic state at elevated temperature (e.g., 250 °C), which may favor oxidation of H_2 and contribute to the observed decrease in CO conversion at high temperature.

In conclusion, we have shown that a Pt shell can be applied to stabilize surface ferrous species. The "FeO-on-Cu@Pt" NPs consisting of Cu@Pt core−shell NPs decorated with surface FeO nanostructures presented similar extraordinary activity and stability in PROX as the FeO-on-Pt/CB catalyst. More importantly, the Pt loading was decreased from 4.0 to <1.0 wt %. The successful fabrication of the highly active Fe/Pt/Cu trimetallic nanocatalyst demonstrates that the "oxide-on-core@shell" catalyst presents a new architecture leading to enhanced catalytic performance with much less usage of noble metals.

■ ASSOCIATED CONTENT

Supporting Information

Experimental methods and Figures S1−S7. This material is available free of charge via the Internet at http://pubs.acs.org.

■ AUTHOR INFORMATION

Corresponding Author

qfu@dicp.ac.cn; xhbao@dicp.ac.cn

Notes

The authors declare no competing financial interest.

■ ACKNOWLEDGMENTS

This work was financially supported by the National Natural Science Foundation of China (11079005, 21103181, 21103171 and 20923001), the Ministry of Science and Technology of China (Grant 2011CBA00503), and the Chinese Academy of Sciences ("Bairen" Program). We acknowledge the fruitful discussions with Dr. Fan Yang.

■ REFERENCES

(1) (a) Green, I. X.; Tang, W.; Neurock, M.; Yates, J. T., Jr. *Science* **2011**, *333*, 736. (b) Qiao, B.; Wang, A.; Yang, X.; Allard, L. F.; Jiang, Z.; Cui, Y.; Liu, J.; Li, J.; Zhang, T. *Nat. Chem.* **2011**, *3*, 634. (c) Ma, C. Y.; Mu, Z.; Li, J. J.; Jin, Y. G.; Cheng, J.; Lu, G. Q.; Hao, Z. P.; Qiao, S. Z. *J. Am. Chem. Soc.* **2010**, *132*, 2608. (d) Fu, Q.; Saltsburg, H.; Flytzani-Stephanopoulos, M. *Science* **2003**, *301*, 935. (e) Liu, H.; Kozlov, A. I.; Kozlova, A. P.; Shido, T.; Iwasawa, Y. *Phys. Chem. Chem. Phys.* **1999**, *1*, 2851.

(2) (a) Tauster, S. J.; Steger, J. J. *J. Catal.* **1990**, *125*, 387. (b) Haller, G. L.; Resasco, D. E. *Adv. Catal.* **1989**, *36*, 62. (c) Chen, M. S.; Goodman, D. W. *Science* **2004**, *306*, 4. (d) Fu, Q.; Wagner, T. *Surf. Sci. Rep.* **2007**, *62*, 431.

(3) (a) Fu, Q.; Wagner, T.; Olliges, S.; Carstanjen, H. D. *J. Phys. Chem. B* **2005**, *109*, 944. (b) Liu, Z.-P.; Jenkins, S.; King, D. *Phys. Rev. Lett.* **2005**, *94*, No. 196102.

(4) (a) Mu, R.; Fu, Q.; Xu, H.; Zhang, H.; Huang, Y.; Jiang, Z.; Zhang, S.; Tan, D.; Bao, X. *J. Am. Chem. Soc.* **2011**, *133*, 1978. (b) Yao, Y.; Fu, Q.; Wang, Z.; Tan, D.; Bao, X. *J. Phys. Chem. C* **2010**, *114*, 17069.

(5) (a) Deng, X.; Lee, J.; Wang, C.; Matranga, C.; Aksoy, F.; Liu, Z. *Langmuir* **2011**, *27*, 2146. (b) Freund, H. J.; Pacchioni, G. *Chem. Soc. Rev.* **2008**, *37*, 2224. (c) Merte, L. R.; Knudsen, J.; Eichhorn, F. M.; Porsgaard, S.; Zeuthen, H.; Grabow, L. C.; Laegsgaard, E.; Bluhm, H.; Salmeron, M.; Mavrikakis, M.; Besenbacher, F. *J. Am. Chem. Soc.* **2011**, *133*, 10692. (d) Netzer, F. P. *Surf. Rev. Lett.* **2002**, *9*, 1553. (e) Netzer, F. P. *Surf. Sci.* **2010**, *604*, 485. (f) Rodriguez, J. A.; Ma, S.; Liu, P.; Hrbek, J.; Evans, J.; Perez, M. *Science* **2007**, *318*, 1757. (g) Xu, L.; Ma, Y.; Zhang, Y.; Jiang, Z.; Huang, W. *J. Am. Chem. Soc.* **2009**, *131*, 16366.

(6) Sun, D.; Gu, X.-K.; Ouyang, R.; Su, H.-Y.; Fu, Q.; Bao, X.; Li, W.-X. *J. Phys. Chem. C* **2012**, *116*, 7491.

(7) Fu, Q.; Li, W.-X.; Yao, Y.; Liu, H.; Su, H.-Y.; Ma, D.; Gu, X.-K.; Chen, L.; Wang, Z.; Zhang, H.; Wang, B.; Bao, X. *Science* **2010**, *328*, 1141.

(8) (a) Mu, R.; Fu, Q.; Liu, H.; Tan, D.; Zhai, R.; Bao, X. *Appl. Surf. Sci.* **2009**, *255*, 7296. (b) Xu, H.; Fu, Q.; Guo, X.; Bao, X. *ChemCatChem* **2012**, DOI: 10.1002/cctc.201200255.

(9) (a) Zhong, C. J.; Maye, M. M. *Adv. Mater.* **2001**, *13*, 1507. (b) Zhang, J.; Lima, F. H. B.; Shao, M. H.; Sasaki, K.; Wang, J. X.; Hanson, J.; Adzic, R. R. *J. Phys. Chem. B* **2005**, *109*, 22701. (c) Yang, H. *Angew. Chem., Int. Ed.* **2011**, *50*, 2674.

(10) (a) Alayoglu, S.; Nilekar, A. U.; Mavrikakis, M.; Eichhorn, B. *Nat. Mater.* **2008**, *7*, 333. (b) Esposito, D. V.; Chen, J. G. *Energy Environ. Sci.* **2011**, *4*, 3900. (c) Jiang, H.-L.; Xu, Q. *J. Mater. Chem.* **2011**, *21*, 13705. (d) Knudsen, J.; Nilekar, A. U.; Vang, R. T.; Schnadt, J.; Kunkes, E. L.; Dumesic, J. A.; Mavrikakis, M.; Besenbacher, F. *J. Am. Chem. Soc.* **2007**, *129*, 6485. (e) Wang, C.; van der Vliet, D.; More, K. L.; Zaluzec, N. J.; Peng, S.; Sun, S.; Daimon, H.; Wang, G.; Greeley, J.; Pearson, J.; Paulikas, A. P.; Karapetrov, G.; Strmcnik, D.; Markovic, N. M.; Stamenkovic, V. R. *Nano Lett* **2011**, *11*, 919.

(11) (a) Plomp, A. J.; van Asten, D. M. P.; van der Eerden, A. M. J.; Maki-Arvela, P.; Murzin, D. Y.; de Jong, K. P.; Bitter, J. H. *J. Catal.* **2009**, *263*, 146. (b) Zhou, C.; Chen, Y.; Guo, Z.; Wang, X.; Yang, Y. *Chem. Commun.* **2011**, *47*, 7473.

(12) Yang, F.; Choi, Y.; Liu, P.; Stacchiola, D.; Hrbek, J.; Rodriguez, J. A. *J. Am. Chem. Soc.* **2011**, *133*, 11474.

(13) Zhou, S.; Varughese, B.; Eichhorn, B.; Jackson, G.; McIlwrath, K. *Angew. Chem., Int. Ed.* **2005**, *44*, 4539.

(14) Liu, X.; Wang, A.; Li, L.; Zhang, T.; Mou, C.-Y.; Lee, J.-F. *J. Catal.* **2011**, *278*, 288.

(15) (a) Xu, H.; Fu, Q.; Yao, Y.; Bao, X. *Energy Environ. Sci.* **2012**, *5*, 6313. (b) Strasser, P.; Koh, S.; Anniyev, T.; Greeley, J.; More, K.; Yu, C.; Liu, Z.; Kaya, S.; Nordlund, D.; Ogasawara, H.; Toney, M. F.; Nilsson, A. *Nat. Chem.* **2010**, *2*, 454.